Malaysian Journal of Mathematical Sciences 17(3): 283–304 (2023)
https://doi.org/10.47836/mjms.17.3.04

Malaysian Journal of Mathematical Sciences

Journal homepage: https://mjms.upm.edu.my

Soret-Dufour Effects on The Waterbased Hybrid Nanofluid Flow with Nanoparticles of Alumina and Copper

Isa, S. S. P. M.*[1,2], Parvin, S. [1], Arifin, N. M. [1,3], Ali, F. M. [1,3], and Ahmad, K. [4]

[1]*Institute for Mathematical Research, Universiti Putra Malaysia, 43400 UPM Serdang, Selangor Darul Ehsan, Malaysia*
[2]*Centre of Foundation Studies for Agricultural Science, Universiti Putra Malaysia, 43400 UPM Serdang, Selangor Darul Ehsan, Malaysia*
[3]*Department of Mathematics and Statistics, Universiti Putra Malaysia, 43400 UPM Serdang, Selangor Darul Ehsan, Malaysia*
[4]*Department of Science in Engineering, Kulliyyah of Engineering, International Islamic University Malaysia, 50728 Gombak, Kuala Lumpur, Malaysia*

E-mail: ctsuzilliana@upm.edu.my
**Corresponding author*

Received: 20 September 2022
Accepted: 11 May 2023

Abstract

The two-dimensional mathematical model of water-based hybrid nanofluid, where the nanoparticles of the model are alumina (Al_2O_3) and copper (Cu) is analyzed in this article. It describes the heat and mass transfer which are induced by concentration and temperature differences, respectively. The current mathematical model extended the works by implementing both directions of moving sheet in the boundary conditions: stretching and shrinking, and use the exponential variations of the sheet velocity, temperature, and concentration of the hybrid nanofluid at the sheet. The final numerical solutions can be obtained by implementing Matlab bvp4c, which involves the step of choosing the most reliable solution in an actual fluid situation. This selection technique on numerical solutions is known as stability analysis and only needs to apply when more than one numerical solution appears in the Matlab bvp4c program. Finally, the controlling parameters such as nanoparticle solid volume fraction, suction, shrinking/stretching, Soret and Dufour cause an increment or decrement in the flow, heat and mass transfer in the hybrid nanofluid. For the stable solution, fluid velocity becomes slower whereas temperature and concentration of the fluid increase when the percentage of Cu, as well as Al_2O_3, rises into the water. Moreover, in case of local Nusselt number and local Sherwood number it is proved that Soret effect is the opposite phenomenon of Dufour effect.

Keywords: hybrid nanofluid; alumina, copper; Soret and Dufour effects; viscous dissipation; Matlab bvp4c; stability analysis.

1 Introduction

Several applications of heat transfer in the fluid flow in the field of engineering and industries require high thermal conductivity. However, regular fluid does not have this feature. To produce better thermal conductivity in the fluid, scientists have proposed to add nanometer-sized particles. This fluid type is known as nanofluid, initially introduced by Choi and Eastman [8]. In recent times, Ghasemian et al. [16] researched with viscoelastic Maxwell/Buongiorno non-Newtonian nanofluid that flows inside a circular cylinder which follows Buongiorno model. Mixed convection and conjugate conduction heat transfer rate of nanofluid applying Manninen's two-phase mixture model experimentally explored by Hoseininejad et al. [19]. However, an upgraded nanofluid is recognized as hybrid nanofluid, and prepared by combining at least 2 nanoparticles into the base fluid. The hybrid type has a higher rate for the most properties compared to the conventional nanofluid, such as thermal conductivity, dispersion stability among particles, Brownian motion among particles, and heat transfer over the fluid and nanoparticles [9]. The main applications of hybrid nanofluid are observed in solar energy devices [25], air conditioning systems [2], heat exchangers [23], and heat pipes [51]. The various types of nanoparticles that occur in hybrid nanofluid are metallic particles, non-metallic particles, and carbon nanotubes [44]. Dinarvand et al.[12], Berrehal et al. [7], and Jabbaripour et al.[22], $MgO - Ag/H_2O$, $Fe_3O_4 - GO/H_2O$, and $Al - Cu/H_2O$ hybrid nanofluid gradually in their study. Saeed Dinarvand [10] experimented with D by using novel hybridity model.

In this research we focused on the well-known hybrid nanofluid $Al_2O_3 - Cu/H_2O$,since their mixture will produce great physical properties of hybrid nanofluid. This is because both nanoparticles have strengths and weaknesses. Alumina has good stability and chemical inertness, but with lower thermal conductivity. Meanwhile, copper possess high thermal conductivity, but with lower stability and reactivity. Therefore, the dispersion of alumina and copper can overcome the weaknesses of both nanoparticles, for the greater function of hybrid nanofluid. The numerical reports of $Al_2O_3 - Cu$/water hybrid nanofluids over a stretching/shrinking surface have been reported: 1) subjected to the convective boundary condition [46], slip condition [6, 26], or thermal radiation [47], 2) represented as mixed convection model [48], and 3) when a magnetic dipole is implemented on hybrid nanofluid [17]. The flow of hybrid $Al_2O_3 - Cu$/water nanofluids in the various geometries also being published, such as rotating plate [13], porous micro-channel [3], convergent/divergent channel [28], and cylinder [15, 20], bricks [20], and platelets [20].

Viscous dissipation is defined as the work done by a fluid on adjacent layers to generate heat, due to the effect of shear forces [34]. This effect is mostly applied to polymer processing known as injection molding [39]. The hybrid nanofluid water-based fluid flow (nanoparticles Al_2O_3 and Cu)over a stretching/shrinking sheet have been investigated [5, 29], subjected to the presence of viscous dissipation. A nonlinear sheet velocity is implemented by Lund et al. [29] specifically on shrinking case. The magnetic field effect was analyzed by Zainal et al. [50] and Aly and Pop [5], for exponential velocity sheet [50] and with the occurrence of stagnation point and partial slip [5]. Besides, the effect of various temperature dependent viscosity for linear sheet velocity have been studied by Venkateswarlu and Satya Narayana [45]. Meanwhile, the heat transfer analysis in $Cu - Al_2O_3/H_2O$ hybrid nanofluid bounded by the various geometries, such as thin needle [27], stretching disk [14], rotational disk [43], circular cylinder [41], and porous channel [4] have been discussed, together with the impact of viscous dissipation. However, another types of nanoparticles (differed from the mixture of Al_2O_3 and Cu) in a hybrid nanofluid have been described, which is affected viscous dissipation. These study relate to the mixture of silver (Ag) and copper (Cu) [24], iron oxide (Fe_3O_4) and cobalt ferrite ($CoFe_2O_4$) [42], copper (Cu) and iron oxide (Fe_3O_4) [30], and silver (Ag) and alumina (Al_2O_3) [33].

Soret and Dufour effects are defined as mass and heat transfer in the fluid flow. The temperature gradient causes changes in concentration, and the mass is transferred (Soret effect). Besides, heat is transferred in the Dufour effect due to the concentration differences. These effects (Soret-Dufour) are coupling process and simultaneous. The numerical studies regarding the Soret-Dufour effects in hybrid nanofluid flow have been published recently [1, 35]. Investigation of stagnation point impact on water based hybrid nanofluid, where Al_2O_3 and Cu are the nanoparticles have been reported by Abad et al. [1]. The model developed by Abad et al. [1] represents the hybrid nanofluid which flows over a cylinder embedded in a porous medium. The water-based hybrid nanomaterials aluminum alloy (AA7075) and titanium alloy (Ti_6Al_4V) were selected by Nisar et al. [35], with the effects of thermal radiation. The model proposed by Nisar et al. [35] is directed stream-wise, together with cross flow. The two nanoparticles (Fe_3O_4 and TiO_2) hybrid nanofluid with transformer oil were described by Raju et al. [38], where two rotating stretched disks bound this nanofluid. The model introduced by Raju et al. [38] was subjected to activation energy and cross-diffusion impacts. Meanwhile, the effects of activation energy and entropy generation on the magnetohydrodynamics methanol-based hybrid nanofluid with nanoparticles SiO_2 and Al_2O_3, bounded by a curved stretching sheet have been studied by Revathi et al. [40].

The application of stability analysis has frequently been used to mathematically validate the solution's reliability. Merkin [32] was the one who first looked into dual solutions and did stability analysis. The upper branch of the solutions was found to be stable, whereas the lower branch was found to be unstable. Weidman et al. [49], on the other hand, investigated the transpiration impact in boundary layer flow past a semi-infinite permeable moving plate. Since they obtained dual numerical solutions, the stability of the solutions is acquired depend on linear disturbances of the steady similarity solutions. After that, several investigations involving the stability analysis in boundary layer flow in a hybrid nanofluids [11, 21] are completed . Recently, Izady et al. [21] and Dinarvand et al. [11] reported with aqueous $Fe_2O_3 - CuO$ and $MgO - Ag$/water hybrid nanofluid gradually considering dual solutions. All of them applied stability analysis and concluded that the solutions are stable when values of the smallest eigenvalue are positive while the solutions are unstable with negative smallest eigenvalue.

From the above literature review, only one team of researchers [35, 40] reported Soret-Dufour coupled parameters' effect on the hybrid nanofluid system bounded by stretching/shrinking sheet. Therefore, this paper fills this gap by inserting the impacts of Soret-Dufour in the mathematical model solved by Lund et al. [29] by implementing the following steps: 1) introduce concentration equation at the governing equation, to express the mathematical formulation of the system, and 2) include the variables which related to the Soret and Dufour parameters in the components of governing equations (energy and concentration) such as mean fluid temperature, thermal diffusion ratio, concentration susceptibility, mass diffusivity, and specific heat at constant pressure. Besides, the current mathematical model in this paper also extended the works by Lund et al. [29] by performing these action: 1) implement both direction of moving sheet in the boundary conditions: stretching and shrinking, instead of only solve shrinking case [29], and 2) use the exponential variations of the velocity, temperature, and concentration of the hybrid nanofluid at the sheet. All of these steps are motivated from the article published by Parvin et al. [36, 37], by substituting the term of Casson fluid to hybrid nanofluid and adding the stability analysis section.

2 Methodology

2.1 Mathematical formulation

A steady two-dimensional model of hybrid nanofluid flow is displayed in Figure 1, where x-axis is placed in vertical vector and y-axis is a horizontal vector. The vector of increasing $+x$-axis is referred to the direction of the stretching sheet, whereas decreasing $+x$-axis is denoted as a direction of shrinking sheet. The sheet velocity is presented as $u = \lambda u_w(x) = \lambda U_0 e^{\frac{x}{L}}$ where $u_w(x)$ is the stretching or shrinking velocity . In the sheet velocity equation, the symbols such as $U_0, L, \lambda > 0$, and $\lambda < 0$ are the reference velocity, reference length, stretching parameter, and shrinking parameter, respectively. The sheet temperature is denoted by $T_w(x) = T_\infty + T_0 e^{\frac{x}{2L}}$ where T_0 is the parameter of the temperature distribution and the adjacent temperature is T_∞. Meanwhile, $C_w(x) = C_\infty + C_0 e^{\frac{x}{2L}}$ where C_0 is the parameter of the concentration distribution and C_∞ indicate the fluid concentration at the sheet and adjacent to it. Copper and alumina nanoparticles are suspended in water (base fluid) and formed $Cu - Al_2O_3/H_2O$ hybrid nanofluid.

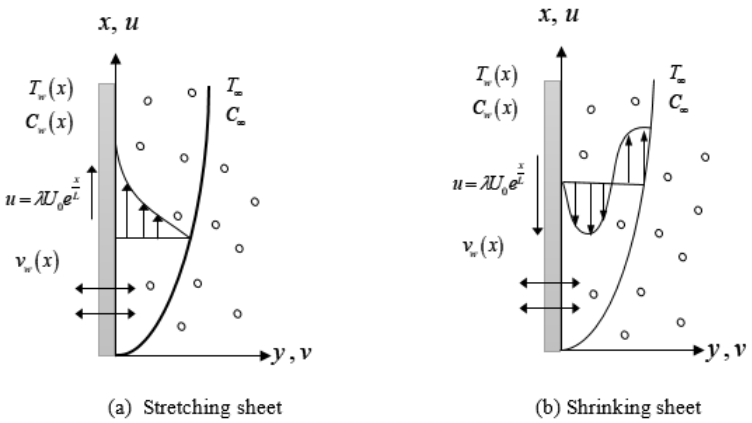

Figure 1: Physical model and coordinate system.

The momentum equation (2) are considered from Waini et al. [46] and Lund et al. [29]. Next, the energy equation (3) is extended from Lund et al. [29] by adding the second-order concentration term along the y-axis at the right side. The concentration equation (4) is taken from Parvin et al. [36, 37]. Therefore, the initial mathematical formulation of the fluid flow model is:

$$\frac{\partial u}{\partial x} + \frac{\partial v}{\partial y} = 0, \tag{1}$$

$$u\frac{\partial u}{\partial x} + v\frac{\partial u}{\partial y} = \frac{\mu_{hnf}}{\rho_{hnf}}\frac{\partial^2 u}{\partial y^2}, \tag{2}$$

$$u\frac{\partial T}{\partial x} + v\frac{\partial T}{\partial y} = \frac{k_{hnf}}{(\rho C_p)_{hnf}}\frac{\partial^2 T}{\partial y^2} + \frac{\mu_{hnf}}{(\rho C_p)_{hnf}}\left(\frac{\partial u}{\partial y}\right)^2 + \frac{D_m K_T}{C_s C_p}\frac{\partial^2 C}{\partial y^2}, \tag{3}$$

$$u\frac{\partial C}{\partial x} + v\frac{\partial C}{\partial y} = D_m\frac{\partial^2 C}{\partial y^2} + \frac{D_m K_T}{T_m}\frac{\partial^2 T}{\partial y^2}, \tag{4}$$

where u, v are the components of velocity in the x, y directions respectively. Other symbols such as D_m, K_T, T, C, C_s, C_p and T_m are denoted as mass diffusivity, thermal diffusion ratio, temperature

of the hybrid nanofluid, concentration of the hybrid nanofluid, concentration susceptibility, specific heat at constant pressure and mean fluid temperature, respectively. Meanwhile, μ_{hnf}, ρ_{hnf}, k_{hnf}, $(\rho C_p)_{hnf}$ characterize the dynamic viscosity, density, thermal conductivity, and heat capacity of the hybrid nanofluid respectively. The derived quantities for hybrid nanofluid are tabulated in Table 1, whereas the related values for the components of the hybrid nanofluid (base fluid and its nanoparticles) are presented in Table 2.

Table 1: The derived quantities of hybrid nanofluid [29, 46, 47, 48].

Properties	**Hybrid nanofluid**
Density	$\rho_{hnf} = \left\{(1-\varphi_2)\left[(1-\varphi_1)+\frac{\varphi_1\rho_{n1}}{\rho_f}\right]+\frac{\varphi_2\rho_{n2}}{\rho_f}\right\}\rho_f$
Heat capacity	$(\rho C_p)_{hnf} = \left\{(1-\varphi_2)\left[(1-\varphi_1)+\frac{\varphi_1(\rho C_p)_{n1}}{(\rho C_p)_f}\right]+\frac{\varphi_2(\rho C_p)_{n2}}{(\rho C_p)_f}\right\}\times(\rho C_p)_f$
Dynamic viscosity	$\mu_{hnf} = \left\{\frac{1}{(1-\varphi_1)^{2.5}(1-\varphi_2)^{2.5}}\right\}\mu_f$
Thermal conductivity	$k_{hnf} = \frac{k_{n2}+2k_{nf}-2\varphi_2(k_{nf}-k_{n2})}{k_{n2}+2k_{nf}+\varphi_2(k_{nf}-k_{n2})}\times\frac{k_{n1}+2k_f-2\varphi_1(k_f-k_{n1})}{k_{n1}+2k_f+\varphi_1(k_f-k_{n1})}\times k_f$

Table 2: The physical values for the base fluid and nanoparticles [29, 46, 47, 48].

Physical properties	**Unit**	**Fluid(water)**	Al_2O_3	**Cu**
Density ρ	kg/m^3	997.1	3970	8933
Specific heat at constant pressure C_p	J/(kg.K)	4179	765	385
Thermal conductivity k	W/(m.K)	0.613	40	400

Here, subscript f, nf, hnf, $n1$, $n2$ indicates the base fluid, nanofluid, hybrid nanofluid, solid component for the first nanofluid, and solid component for the second nanofluid respectively. Also, φ_1 and φ_2 are the volume fractions of Al_2O_3 and Cu nanoparticles respectively.

The appropriate boundary conditions are:

At the sheet $y = 0$:

$$u = \lambda u_w(x) = \lambda U_0 e^{\frac{x}{L}}, \quad v = v_w(x) = \left[-\left(\frac{vU_0}{2L}\right)^{\frac{1}{2}} e^{\frac{x}{2L}}\right] S,$$
$$T_w(x) = T_\infty + T_0 e^{\frac{x}{2L}}, \quad C_w(x) = C_\infty + C_0 e^{\frac{x}{2L}}. \tag{5}$$

Far from the sheet as $y \to \infty$,

$$u \to 0, \quad T \to T_\infty, \quad C \to C_\infty,$$

where S is the suction parameter, $v_w(x)$ is the mass transfer velocity and v_f is the kinematic viscosity of the base fluid.

The related similarity variables are represented as [36, 37]:

$$\eta = y\left(\frac{U_0}{2\upsilon_f L}\right)^{\frac{1}{2}} e^{\frac{x}{2L}}, \quad \theta(\eta) = \frac{T-T_\infty}{T_w-T_\infty}, \quad \phi(\eta) = \frac{C-C_\infty}{C_w-C_\infty},$$
$$\psi(x,y) = (2\upsilon_f L U_0)^{\frac{1}{2}} e^{\frac{x}{2L}} f(\eta) \quad \text{where} \quad u = \frac{\partial\psi}{\partial y}, \quad v = -\frac{\partial\psi}{\partial x}, \tag{6}$$

where $\psi = (x, y)$ denotes the stream function.

The equation equation (6) is substituted into equations (2) - (5) to obtain the following equations:

$$\left(\frac{\mu_{hnf}}{\mu_f} \times \frac{\rho_f}{\rho_{hnf}}\right)\left(f'''(\eta)\right) - 2\left(f'(\eta)\right)^2 + f(\eta)f''(\eta) = 0, \tag{7}$$

$$\frac{(\rho C_p)_f}{(\rho C_p)_{hnf}} \times \left[\left(\frac{1}{Pr}\right)\left(\frac{k_{hnf}}{k_f}\right)\theta''(\eta) + \left(\frac{\mu_{hnf}}{\mu_f}\right)(Ec)\left(f''(\eta)\right)^2\right] \\ -f'(\eta)\theta(\eta) + f(\eta)\theta'(\eta) + Db\left(\phi''(\eta)\right) = 0, \tag{8}$$

$$\frac{1}{Sc}\phi''(\eta) + Sr\theta''(\eta) - f'(\eta)\phi(\eta) + f(\eta)\phi'(\eta) = 0, \tag{9}$$

and

$$f'(\eta) = \lambda, \quad f(\eta) = S, \quad \theta(\eta) = 1, \quad \phi(\eta) = 1, \quad \text{when} \quad \eta = 0,$$
$$f'(\eta) \to 0, \quad \theta(\eta) \to 0, \quad \phi(\eta) \to 0, \quad \text{when} \quad \eta \to \infty. \tag{10}$$

The parameters involved in this model are presented in Table 3:

Table 3: List of governing parameters.

Mathematical Formulation	**Name**
$Pr = \dfrac{\mu_f (C_p)_f}{k_f}$	Prandtl number
$Sc = \dfrac{\upsilon_f}{D_m}$	Schmidt number
$Sr = \dfrac{D_m K_T (T_w - T_\infty)}{T_m \upsilon_f (C_w - C_\infty)}$	Soret number
$Db = \dfrac{D_m K_T (C_w - C_\infty)}{C_s C_p \upsilon_f (T_w - T_\infty)}$	Dufour number
$Ec = \dfrac{U_0^2}{C_p (T_w - T_\infty)}$	Eckert number

The physical quantities namely as skin friction coefficient C_f, local Nusselt number Nu_x and

local Sherwood number Sh_x are defined as:

$$\begin{aligned} C_f &= \frac{\mu_{hnf}}{\rho_f U_0^2}\left(\frac{\partial u}{\partial y}\right)_{y=0}, \\ Nu_x &= \frac{-Lk_{hnf}}{k_f(T_w - T_\infty)}\left(\frac{\partial T}{\partial y}\right)_{y=0}, \\ Sh_x &= \frac{\rho_{hnf}}{\rho_f}\frac{L}{(C_w - C_\infty)}\left(-\frac{\partial C}{\partial y}\right)_{y=0}. \end{aligned} \tag{11}$$

Using equation (6) into equation (11), we obtain,

$$\begin{aligned} C_f\sqrt{2Re_x}e^{-\frac{2x}{L}} &= \frac{\mu_{hnf}}{\mu_f}f''(0), \\ Nu_x\sqrt{\frac{2}{Re_x}} &= -\frac{k_{hnf}}{k_f}\theta'(0), \\ Sh_x\sqrt{\frac{2}{Re_x}} &= -\frac{\rho_{hnf}}{\rho_f}\phi'(0), \end{aligned} \tag{12}$$

where $Re_x = \dfrac{LU_0}{\upsilon_f}e^{\frac{x}{L}}$ is the Reynolds number.

2.2 Stability analysis

Dual solutions for the above equations have been obtained for certain values of the parameters as in Table 3. Therefore, the most stable numerical solution over time is selected by performing a temporal stability analysis. So, the unsteady state for initial mathematical formulation are as follow:

$$\frac{\partial u}{\partial t} + u\frac{\partial u}{\partial x} + v\frac{\partial u}{\partial y} = \frac{\mu_{hnf}}{\rho_{hnf}}\frac{\partial^2 u}{\partial y^2}, \tag{13}$$

$$\frac{\partial T}{\partial t} + u\frac{\partial T}{\partial x} + v\frac{\partial T}{\partial y} = \frac{k_{hnf}}{(\rho C_p)_{hnf}}\frac{\partial^2 T}{\partial y^2} + \frac{\mu_{hnf}}{(\rho C_p)_{hnf}}\left(\frac{\partial u}{\partial y}\right)^2 + \frac{D_m K_T}{C_s C_p}\frac{\partial^2 C}{\partial y^2}, \tag{14}$$

$$\frac{\partial C}{\partial t} + u\frac{\partial C}{\partial x} + v\frac{\partial C}{\partial y} = D_m\frac{\partial^2 C}{\partial y^2} + \frac{D_m K_T}{T_m}\frac{\partial^2 T}{\partial y^2}. \tag{15}$$

A non-dimensional time variable τ is introduced [49] in the new similarity variables:

$$\begin{aligned} &\theta(\eta,\tau) = \frac{T - T_\infty}{T_w - T_\infty}, \qquad \phi(\eta,\tau) = \frac{C - C_\infty}{C_w - C_\infty}, \qquad \psi(x,y) = (2\upsilon_f LU_0)^{\frac{1}{2}}e^{\frac{x}{2L}}f(\eta,\tau), \\ &\eta = y\left(\frac{U_0}{2\upsilon_f L}\right)^{\frac{1}{2}}e^{\frac{x}{2L}}, \qquad \tau = \frac{U_0 t}{2L}e^{\frac{x}{L}}, \qquad u = U_0 e^{\frac{x}{L}}\frac{\partial}{\partial\eta}f(\eta,\tau), \\ &v = -\frac{U_0}{2L}ye^{\frac{x}{L}}\frac{\partial}{\partial\eta}f(\eta,\tau) - \frac{1}{2L}(2\upsilon_f LU_0)^{\frac{1}{2}}\left[\frac{U_0}{L}te^{\frac{3x}{2L}}\frac{\partial}{\partial\tau}f(\eta,\tau) + e^{\frac{x}{2L}}f(\eta,\tau)\right]. \end{aligned} \tag{16}$$

The substitution of equation (16) into equations (13) - (15) produce:

$$\left(\frac{\mu_{hnf}}{\mu_f}\right)\left(\frac{\rho_f}{\rho_{hnf}}\right)\left(\frac{\partial^3 f}{\partial\eta^3}\right) + 2\tau\left[\frac{\partial f}{\partial\tau}\frac{\partial^2 f}{\partial\eta^2} - \frac{\partial f}{\partial\eta}\frac{\partial^2 f}{\partial\eta\partial\tau}\right] + f\frac{\partial^2 f}{\partial\eta^2} - \frac{\partial^2 f}{\partial\eta\partial\tau} - 2\left(\frac{\partial f}{\partial\eta}\right)^2 = 0, \tag{17}$$

$$\frac{(\rho C_p)_f}{(\rho C_p)_{hnf}} \times \left[\left(\frac{k_{hnf}}{k_f}\right)\left(\frac{1}{Pr}\right)\frac{\partial^2\theta}{\partial\eta^2} + Ec\left(\frac{\mu_{hnf}}{\mu_f}\right)\left(\frac{\partial^2 f}{\partial\eta^2}\right)^2\right] + 2\tau\left[\frac{\partial f}{\partial\tau}\frac{\partial\theta}{\partial\eta} - \frac{\partial f}{\partial\eta}\frac{\partial\theta}{\partial\tau}\right] + f\frac{\partial\theta}{\partial\eta} - \theta\frac{\partial f}{\partial\eta} - \frac{\partial\theta}{\partial\tau} + Db\frac{\partial^2\phi}{\partial\eta^2} = 0, \tag{18}$$

$$\left(\frac{1}{Sc}\right)\frac{\partial^2\phi}{\partial\eta^2} + 2\tau\left[\frac{\partial f}{\partial\tau}\frac{\partial\phi}{\partial\eta} - \frac{\partial f}{\partial\eta}\frac{\partial\phi}{\partial\tau}\right] - \frac{\partial\phi}{\partial\tau} + f\frac{\partial\phi}{\partial\eta} - \phi\frac{\partial f}{\partial\eta} + Sr\frac{\partial^2\theta}{\partial\eta^2} = 0, \tag{19}$$

with boundary conditions:

$$\begin{aligned} &\frac{\partial f}{\partial\eta}(\eta,\tau) = \lambda, \quad f(\eta,\tau) = S, \quad \theta(\eta,\tau) = 1, \quad \phi(\eta,\tau) = 1, \quad \text{at} \quad \eta = 0, \\ &\frac{\partial f}{\partial\eta}(\eta,\tau) \to 0, \quad \theta(\eta,\tau) \to 0, \quad \phi(\eta,\tau) \to 0, \quad \text{as} \quad \eta \to \infty. \end{aligned} \tag{20}$$

Following Weidman et al. [49] to determine the steady flow, we take

$$\begin{aligned} f(\eta,\tau) &= f_0(\eta) + e^{-\gamma\tau}F(\eta,\tau), \\ \theta(\eta,\tau) &= \theta_0(\eta) + e^{-\gamma\tau}G(\eta,\tau), \\ \phi(\eta,\tau) &= \phi_0(\eta) + e^{-\gamma\tau}H(\eta,\tau), \end{aligned} \tag{21}$$

where γ denotes an unknown eigenvalue, and $F(\eta,\tau)$, $G(\eta,\tau)$ and $H(\eta,\tau)$ are small relative to $f_0(\eta)$, $\theta_0(\eta)$ and $\phi_0(\eta)$. Next, we substitute equation (21) into equation (17) - (19) and set $\tau = 0$. As a result, the following equations are obtained:

$$\left(\frac{\mu_{hnf}}{\mu_f}\right) \times \left(\frac{\rho_f}{\rho_{hnf}}\right) F''' + f_0F'' + Ff_0'' + \gamma F' - 4f_0'F' = 0, \tag{22}$$

$$\frac{(\rho C_p)_f}{(\rho C_p)_{hnf}} \times \left[\left(\frac{k_{hnf}}{k_f}\right)\left(\frac{1}{Pr}\right)G'' + 2Ec\left(\frac{\mu_{hnf}}{\mu_f}\right)f_0''F''\right] + f_0G' - Gf_0' + F\theta_0' - \theta_0F' + \gamma G + (Db)H'' = 0, \tag{23}$$

$$\frac{1}{Sc}H'' + f_0H' - Hf_0' + \phi_0'F - \phi_0F' + \gamma H' + SrG'' = 0. \tag{24}$$

The boundary conditions are:

At $\eta = 0$,

$$F'(0,\tau) = 0, \quad F(0,\tau) = 0, \quad G(0,\tau) = 0, \quad H(0,\tau) = 0.$$

As $\eta \to \infty$,

$$F'(\eta,\tau) \to 0, \quad G(\eta,\tau) \to 0, \quad H(\eta,\tau) \to 0. \tag{25}$$

The initial boundary condition $F'(\eta,\tau) \to 0$ as $\eta \to \infty$ is relaxed for the recent problem. Previous researchers [18] have described the relaxation strategy for boundary conditions. Lastly, the equations (22) - (24) together with the new boundary condition $F_0''(0) = 1$ are calculated using Matlab bvp4c program.

3 Results and Discussion

Transformed ordinary differential equations (7) to (9) along with the boundary condition (10) produce numerical solutions through Matlab bvp4c solver. The assumption of the initial guess value and the boundary layer thickness, η with the various values of the parameters are employed to find the required solutions. The impact of first nanoparticles solid volume fraction φ_1 second nanoparticles solid volume fraction φ_2, Soret number Sr, and Dufour number, Db are displayed by velocity $f'(\eta)$ temperature $\theta(\eta)$ or concentration profile $\phi(\eta)$ as well as, skin friction coefficient $C_f\sqrt{2Re_x}e^{-\frac{2x}{L}}$, local Nusselt number $Nu_x\sqrt{2/Re_x}$, or local Sherwood number $Sh_x\sqrt{2/Re_x}$. In the current study, boundary layer thickness $\eta = 10$ is considered for velocity profile and $\eta = 15$ is chosen in the case of temperature and concentration profiles. The volume fraction of Al_2O_3 nanoparticles $\varphi_1 = 0.1$, volume fraction of Cu nanoparticles $\varphi_2 = 0.4$ suction parameter $S = 4.0$, shrinking parameter $\lambda = -1.0$, Soret number $Sr = 0.2$, Schmidt number $Sc = 0.1$, Dufour number $Db = 2.5$, Eckert number $Ec = 0.2$, Prandtl number $Pr = 2.0$ are considered unless otherwise declared. In this research, primarily, the nanoparticle of Al_2O_3 is added to the water with a 0.1 solid volume fraction. Subsequently, Cu is added with 0.4 solid volume fractions to form the Cu-Al_2O_3/water hybrid nanofluid. Besides, Coper and alumina are mixed with water in different ratios ($0 \leq \varphi_1 \leq 0.425$ and $0 \leq \varphi_2 \leq 0.65$).

Table 4 shows a comparison of the current data with previously published literature [48, 31] for the validation of the current model. In the current research, the physical quantities $f''(0)$ decrease with the increasing S which is in great agreement with prior researchers. Table 5 is also created in order to validate the outcomes of the heat transfer rate for Al_2O_3 - Cu/water hybrid nanofluid for several values of suction parameters, first and second nanoparticles volume fraction. The results of the current study are compared to the results of Lund et al. [29] and found in excellent agreement.

Table 4: Values of $f''(0)$ against S when $Sr = Db = Ec = Sc = 0.0$, $Pr = 6.2$, $\phi_1 = \phi_2 = 0$ (regular fluid) and $\lambda = 1$(stretching case).

S	$f''(0)$		
	Magyari and Keller [31] (shooting method)	Waini et al.[48] (bvp4c Matlab)	Present (bvp4c Matlab)
0	-1.281808	-1.28181	-1.28180
1		-1.84983	-1.84987
2			-2.60484
3			-3.44528

Table 5: Values of $-\theta'(0)$ over the shrinking surface ($\lambda = -1.5$) and $Pr = 6.2$, $Ec = 0.1$ for different values of S, ϕ_1 and ϕ_2.

S	ϕ_1 (Cu water)	ϕ_2 (Al_2O_3 water)	$-\theta(0)$	
			Lund et al. [29]	Present
3.4518	0.10	0.10	8.330535	8.330536
3.1715	0.10	0.00	11.664798	11.664789
3.3031	0.05	0.05	11.769647	11.769645
3.3021	0.01	0.05	13.612244	13.612249
3.3022	0.00	0.05	14.123427	14.123467

The effect of $C_f\sqrt{2Re_x}e^{-\frac{2x}{L}}$, $Nu_x\sqrt{2/Re_x}$ and $Sh_x\sqrt{2/Re_x}$ againts $\lambda < 0$ and $\lambda > 0$ for different ϕ_2 values are illustrated in Figures 2 - 4. For the second solution, $C_f\sqrt{2Re_x}e^{-\frac{2x}{L}}$ (Figure 2) $Nu_x\sqrt{2/Re_x}$ (Figure 3) decrease and $Sh_x\sqrt{2/Re_x}$ (Figure 4) increases with the rise of ϕ_2. At the same time, the first solution of $Nu_x\sqrt{2/Re_x}$ declined and $Sh_x\sqrt{2/Re_x}$ inclined with inclined ϕ_2, but dual behaviors are observed for $C_f\sqrt{2Re_x}e^{-\frac{2x}{L}}$. The variation of $C_f\sqrt{2Re_x}e^{-\frac{2x}{L}}$ declines in the stretching area $(\lambda > 0)$ and is inclined to the shrinking area $(\lambda < 0)$ (Figure 2). Moreover, in three Figures 2 - 4, all the critical point exists in the shrinking region $(\lambda < 0)$, namely $\lambda_1 = -3.6201$, $\lambda_2 = -3.802$ and $\lambda_3 = -3.9$ for $\phi_2 = 0.05, 0.1$ and 0.2 respectively. On both branch solutions, the values of $C_f\sqrt{2Re_x}e^{-\frac{2x}{L}}$ are larger in the shrinking zone $(\lambda > 0)$ than in the stretching zone $(\lambda < 0)$, as shown in Figure 2.

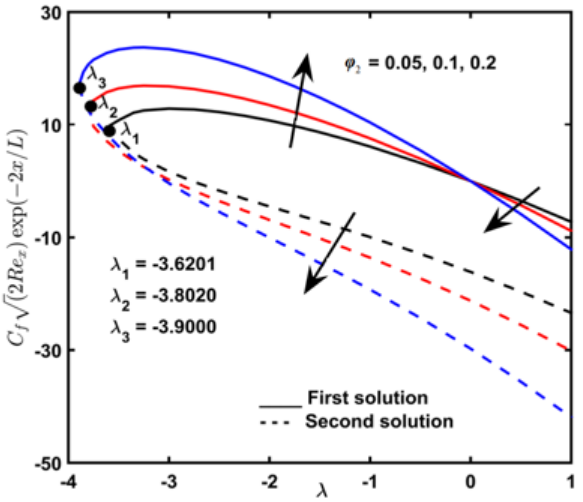

Figure 2: Effect of ϕ_2 and λ on $C_f\sqrt{2Re_x}e^{-\frac{2x}{L}}$.

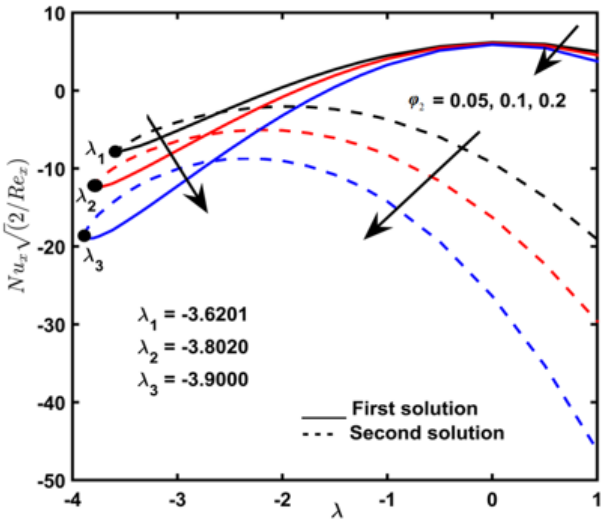

Figure 3: Effect of ϕ_2 and λ on $Nu_x\sqrt{2/Re_x}$.

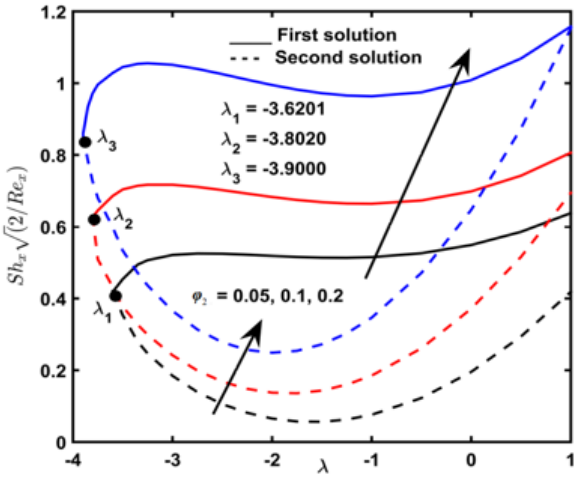

Figure 4: Effect of ϕ_2 and λ on $Sh_x\sqrt{2/Re_x}$.

Figures 5 and 6 describe the variations of $Nu_x\sqrt{2/Re_x}$ and $Sh_x\sqrt{2/Re_x}$ against Db parameter for three different values of Sr. It is noticed from Figure 5 that the first solution of $Nu_x\sqrt{2/Re_x}$ slightly increased near the sheet and decreased for large Db with enhancing Sr, whereas the second solution decreased in all the range of Db. Both solutions in $Nu_x\sqrt{2/Re_x}$ continuously go down with the augmentation of Db (Figure 5). On the other hand, both solutions act oppositely in Figure 6 compare to Figure 5. The reason is that Db (diffusion-thermo) is the opposite phenomenon of Sr (thermal diffusion). The first solution of $Sh_x\sqrt{2/Re_x}$ goes down for small Db and reverse for large Db with the addition of Sr while the second solution goes up for all the values of Db (Figure 6).

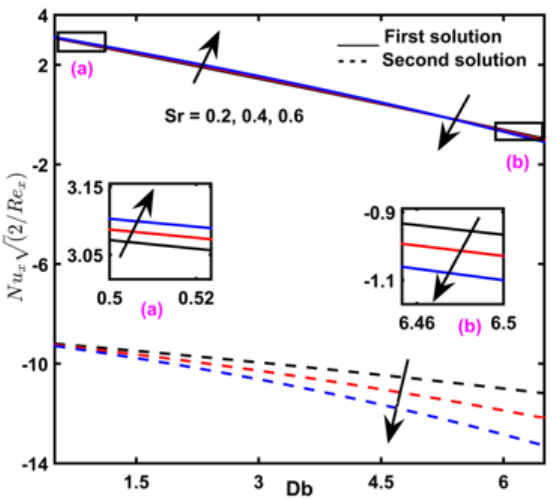

Figure 5: Effect of Db and Sr on $Nu_x\sqrt{2/Re_x}$.

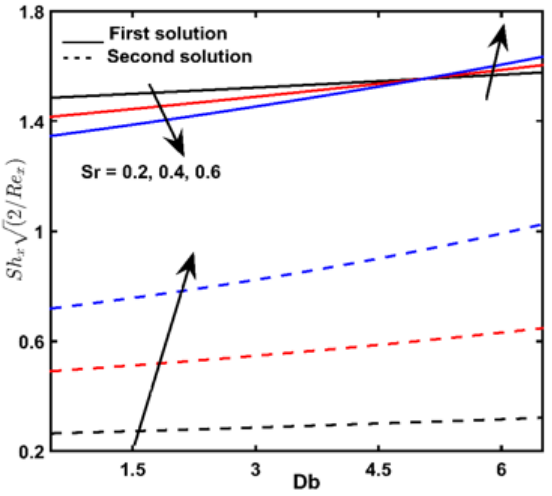

Figure 6: Effect of Db and Sr on $Sh_x\sqrt{2/Re_x}$.

The $f'(\eta)$ profiles are presented for different values of ϕ_1 (Figure 7) and ϕ_2 (Figure 8). All the profiles asymptotically satisfy the boundary conditions (equation 10), indicating that the numerical results are valid. There is no fluid velocity for the bigger boundary layer thickness ($\eta \to \infty$). So, the fluid becomes stable as it goes far from the wall. In Figures 7 and 8, the growth in ϕ_1 and ϕ_2 led to the decrement of the velocity (first solution). Therefore, fluid velocity becomes slower when the percentage of Cu, as well as Al_2O_3 rises into the water. With the increment of nanoparticles, velocity falls, indicating that mass movement is slower, which may have an adverse influence on heat transport. The second solution inclined near the wall for both figures 7 and 8 and eventually its behavior becomes opposite for growing boundary layer thickness. In two cases (Figure 7 and 8), for the second solution minimum peak exists near the wall and gradually it increases up to zero value for large η ($\eta \to \infty$).

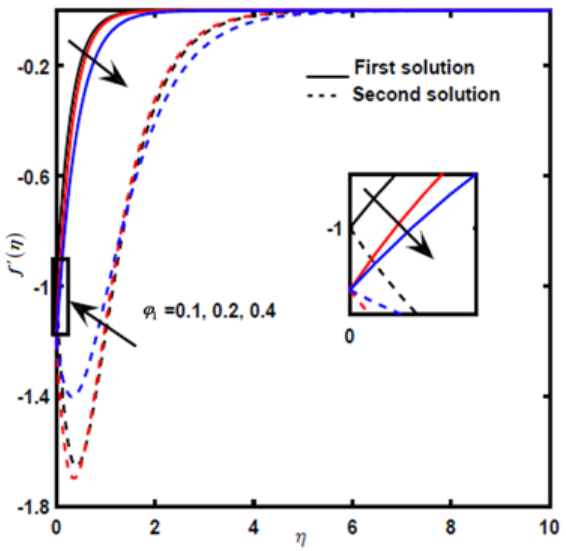

Figure 7: The $f'(\eta)$ profile for various values of ϕ_1.

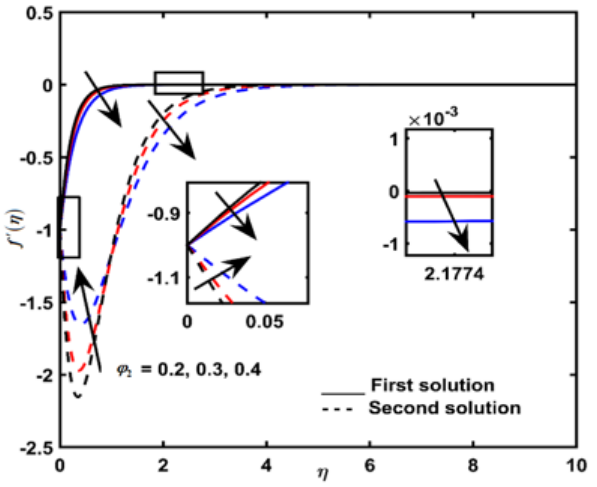

Figure 8: The $f'(\eta)$ profile for various values of ϕ_2.

Figures 9 to 12 show the $\theta(\eta)$ profiles for various values of different parameters against η. The field of $\theta(\eta)$ is portrayed due to the governing parameters ϕ_1 (Figure 9), ϕ_2 (Figure 10), Db (Figure 11) and Sr (Figure 12). In Figures 9 and 10, when the velocity ratio parameters ϕ_1, and ϕ_2 are increased, the fluid velocity rises (for the stable solution). The second solution declined near the shrinking sheet and reverse when far from the sheet (Figures 9 and 10). Moreover, with increasing Db, the fluid velocity goes up for both solutions (Figure 11). Large Db raises the temperature and thickness of the thermal layer (Figure 11). Increment of Dufour number decrease the thermal resistance which lead to the addition of the surface temperature. However, Soret number Sr causes the temperature of the first solution to reduce at the smaller thermal boundary layer thickness, and it changes its pattern at the thicker thermal boundary layer thickness (Figure 12). In all cases, the second solution reaches the maximum point for the concentration profiles when it is very close to the sheet (Figure 9 to 12) and fell gradually with the distance from the sheet ($\eta \to \infty$).

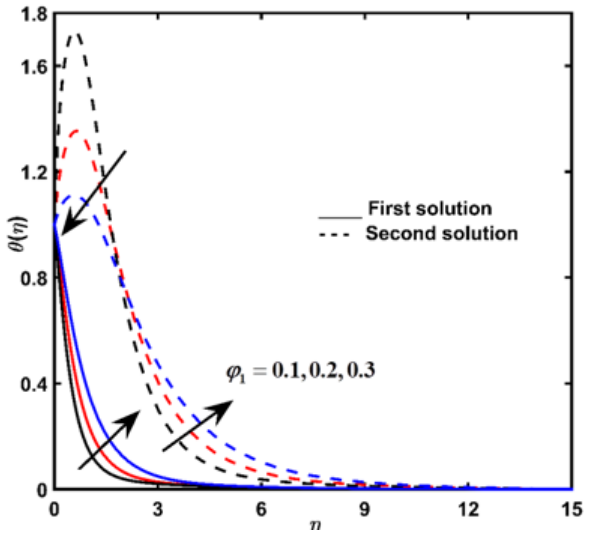

Figure 9: The $\theta(\eta)$ profile against ϕ_1.

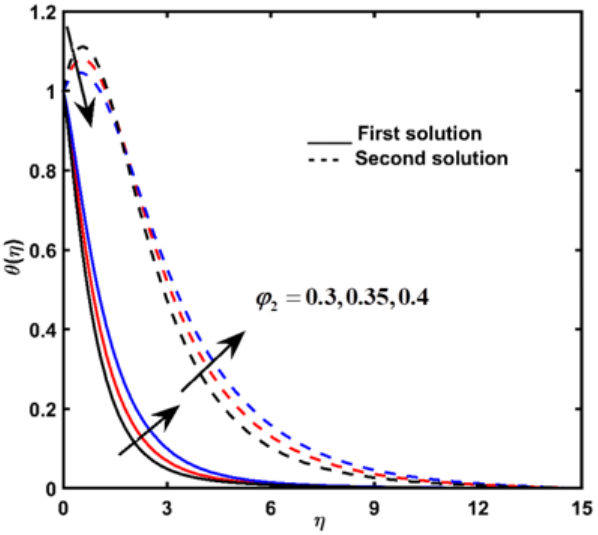

Figure 10: The $\theta(\eta)$ profile against ϕ_2.

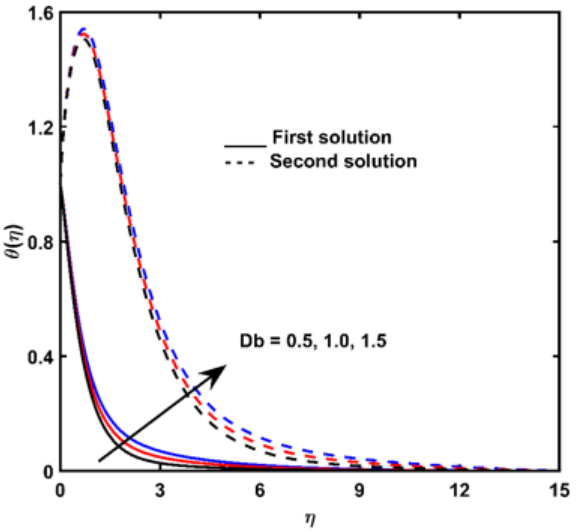

Figure 11: The $\theta(\eta)$ profile against Db.

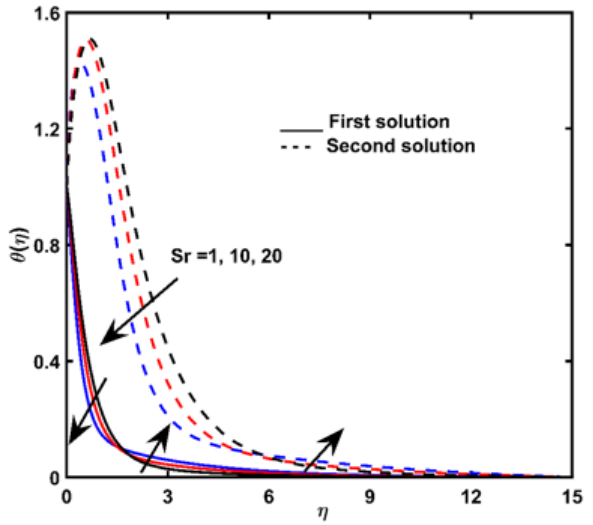

Figure 12: The $\theta(\eta)$ profile against Sr.

Figures 13 - 15 show the $\phi(\eta)$ profiles for several physical parameters such as φ_1, φ_2, and Sr respectively. In all the figures, it is noticed that the fluid concentration is high at the sheet $(y = 0)$ and gradually it decreases until goes to zero. So there is no concentration effect for large boundary layer thickness $(\eta \to \infty)$ which satisfies the boundary condition (equation 10). From Figures 13 - 15, it is clear that when the percentage of first and second nanoparticles solid volume fraction (φ_1 and φ_2 and Sr increase, then the fluid concentration of the first solution also increases. However, it acts oppositely for the second solution for the parameter φ_1 and φ_2 (Figures 13 and 14). For the effect of Sr, dual behavior was observed for the second solution (Figure 15), where fluids concentration becomes lesser near the wall and after a short distance, it started to increase with the increment of Sr. As the value of Sr rises, the fluid concentration rises due to the role of temperature gradients in species diffusion.

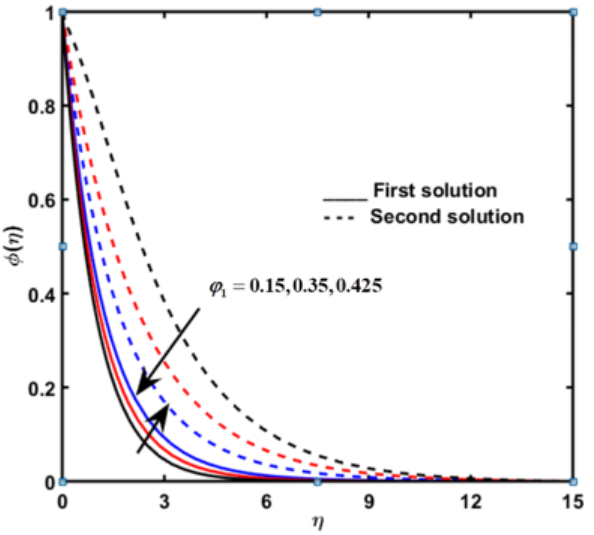

Figure 13: The $\phi(\eta)$ profile against ϕ_1.

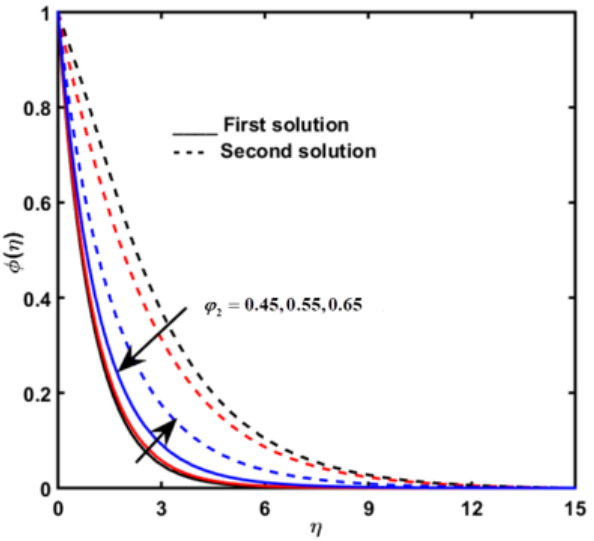

Figure 14: The $\phi(\eta)$ profile against ϕ_2.

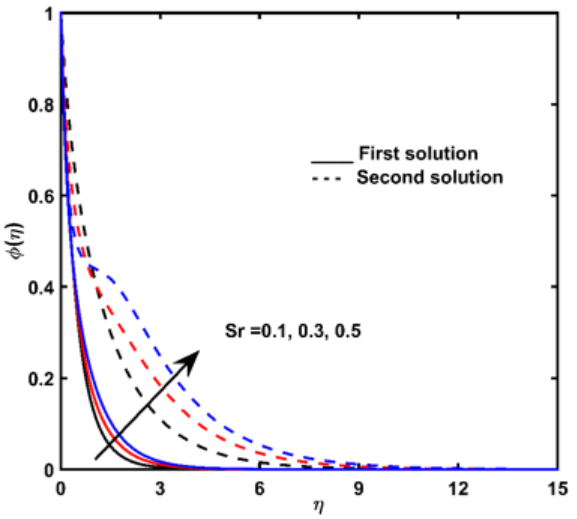

Figure 15: The $\phi(\eta)$ profile against Sr.

Figure 16 illustrates the smallest eigenvalues γ against λ when $Pr = 0.2$, $S = 0.4$, $\varphi_1 = 0.05$, $\varphi_2 = 0.4$. As mentioned in equation (21), the decrement of disturbance for increasing time causes the fluid flow becomes stable. Meanwhile, the flow is unstable for the increment of disturbance. The region of $\gamma > 0$ makes the flow stable whereas fluids flow is unstable when $\gamma < 0$. Figure 16 shows that the first solution is stable and the second solution is unstable and rejected. Also, when $\gamma \to 0$ both solutions go to the critical point ($\lambda_c = -3.6201$).

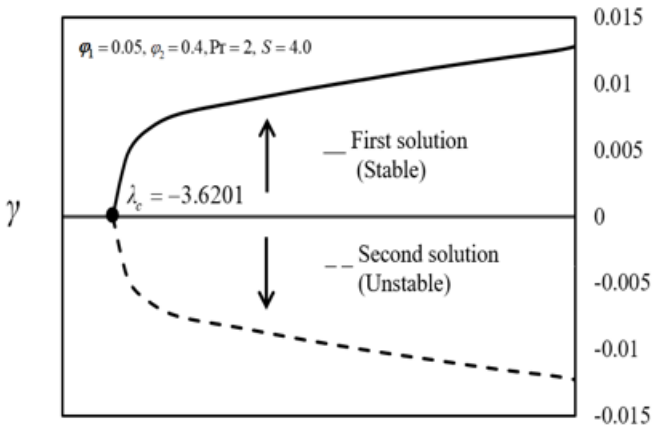

Figure 16: Graph of the γ variation for different values of $\lambda < 0$.

.

4 Conclusion

Boundary layer flow and heat transfer of a hybrid nanofluid $(Cu - Al_2O_3/H2_O)$ over a permeable exponentially shrinking and stretching sheet is investigated. The main findings are listed as below:

1. The validity of the current work is established by comparing the current results with previous researchers, and good agreement is observed.
2. The first solution of skin friction coefficient and both branch solutions of local Sherwood number increase with the increment of the second nanoparticles volume fraction. Both solutions of local Nusselt number and unstable solution of skin friction coefficient goes down with the rise of the same parameter.
3. Both branch solution of local Nusselt number and the second solution of skin friction coefficient decreased with the rising values of second nanoparticles in the presence of shrinking and stretching sheet whereas both branch solution of local Sherwood number increase.
4. A reverse trend is observed for the local Nusselt number and local Sherwood number for both solutions with the augmentation of Soret number and stretching/shrinking parameter.
5. For the first solution, the temperature of the fluid increase with the increment of both nanoparticles and Dufour number. Dual behavior for Soret number is observed for the temperature profile.
6. The concentration of the fluid augmented with raising both nanoparticles and Soret number for the stable solution.
7. Checking of stability confirmed that only the first solution is stable and the second solution is unstable.

5 Future Direction

In the future, the additional controlling parameters may be introduced in the present fluid flow model. Moreover, the implementation of different nanoparticles with the higher heat transfer rate can be considered, to find out which nanoparticles can achieve better thermal performance.

Acknowledgement The present research was supported by Ministry of Education Malaysia through Fundamental Research Grant Scheme FRGS/1/2020/STG06/UPM/02/1.

Conflicts of Interest The authors declare that there is no conflict of interest.

References

[1] J. M. N. Abad, R. Alizadeh, A. Fattahi, M. H. Doranehgard, E. Alhajri & N. Karimi (2020). Analysis of transport processes in a reacting flow of hybrid nanofluid around a bluff-body embedded in porous media using artificial neural network and particle swarm optimization. *Journal of Molecular Liquids*, *313*, 113492. https://doi.org/10.1016/j.molliq.2020.113492.

[2] M. S. Ahmed & A. M. Elsaid (2019). Effect of hybrid and single nanofluids on the performance characteristics of chilled water air conditioning system. *Applied Thermal Engineering*, *163*, Article ID 114398. https://doi.org/10.1016/j.applthermaleng.2019.114398.

[3] Z. Alhajaj, M. Z. Saghir & M. M. Rahman (2019). Convective heat transfer of mono and hybrid nanofluid in porous micro-channel: Experimental and numerical approach. *Excerpt from the Proceedings of the 2019 COMSOL Conference in Boston*,. https://www.comsol.com/paper/convective-heat-transfer-of-mono-and-hybrid-nanofluid-in-porous-micro-channel-ex-80801.

[4] A. Ali, A. Noreen, S. Saleem, A. Aljohani & M. Awais (2021). Heat transfer analysis of $Cu - Al_2O_3$ hybrid nanofluid with heat flux and viscous dissipation. *Journal of Thermal Analysis and Calorimetry*, *143*(3), 2367–2377. https://doi.org/10.1007/s10973-020-09910-6.

[5] E. H. Aly & I. Pop (2020). MHD flow and heat transfer near stagnation point over a stretching/shrinking surface with partial slip and viscous dissipation: Hybrid nanofluid versus nanofluid. *Powder Technology*, *367*, 192–205. https://doi.org/10.1016/j.powtec.2020.03.030.

[6] S. A. Bakar, N. M. Arifin, N. Bachok & F. M. Ali (2022). Hybrid nanofluid flow in a porous medium with second-order velocity slip, suction and heat absorption. *Malaysian Journal of Mathematical Sciences*, *16*(2), 257–272. https://doi.org/10.47836/mjms.16.2.06.

[7] H. Berrehal, S. Dinarvand & I. Khan (2022). Mass-based hybrid nanofluid model for entropy generation analysis of flow upon a convectively-warmed moving wedge. *Chinese Journal of Physics*, *77*, 2603–2616. https://doi.org/10.1016/j.cjph.2022.04.017.

[8] S. U. Choi & J. A. Eastman. Enhancing thermal conductivity of fluids with nanoparticles. Technical report Argonne National Laboratory, Argonne, IL (United States) 1995. https://www.osti.gov/biblio/196525.

[9] S. U. Choi. Nanofluids: A new field of scientific research and innovative applications 2008. https://doi.org/10.1080/01457630701850778.

[10] S. Dinarvand (2019). Nodal/saddle stagnation-point boundary layer flow of $CuO-Ag$/water hybrid nanofluid: a novel hybridity model. *Microsystem Technologies*, *25*(7), 2609–2623. https://doi.org/10.1007/s00542-019-04332-3.

[11] S. Dinarvand, S. M. Mousavi, M. Yousefi & M. Nademi Rostami (2022). MHD flow of $MgO-Ag$/water hybrid nanofluid past a moving slim needle considering dual solutions: An applicable model for hot-wire anemometer analysis. *International Journal of Numerical Methods for Heat & Fluid Flow*, *32*(2), 488–510. https://doi.org/10.1108/HFF-01-2021-0042.

[12] S. Dinarvand & A. M. Nejad (2021). Off-centered stagnation point flow of an experimental-based hybrid nanofluid impinging to a spinning disk with low to high non-alignments. *International Journal of Numerical Methods for Heat & Fluid Flow*, *32*(8), 2799–2818. https://doi.org/10.1108/HFF-09-2021-0637.

[13] M. R. Eid (2022). 3-D flow of magnetic rotating hybridizing nanoliquid in parabolic trough solar collector: Implementing Cattaneo-Christov heat flux theory and Centripetal and Coriolis forces. *Mathematics*, *10*(15), 2605. https://doi.org/10.3390/math10152605.

[14] U. Farooq, M. I. Afridi, M. Qasim & D. Lu (2018). Transpiration and viscous dissipation effects on entropy generation in hybrid nanofluid flow over a nonlinear radially stretching disk. *Entropy*, *20*(9), 668. https://doi.org/10.3390/e20090668.

[15] K. Gangadhar, D. N. Bhargavi, T. Kannan, M. Venkata Subba Rao & A. J. Chamkha (2020). Transverse MHD flow of Al_2O_3-Cu/H_2O hybrid nanofluid with active radiation: a novel hybrid model. *Mathematical Methods in the Applied Sciences*, pp. 1–19. https://doi.org/10.1002/mma.6671.

[16] A. Ghasemian, S. Dinarvand, A. Adamian & M. A. Sheremet (2019). Unsteady general three-dimensional stagnation point flow of a Maxwell/Buongiorno non-Newtonian nanofluid. *Journal of Nanofluids*, *8*(7), 1544–1559. https://doi.org/10.1166/jon.2019.1701.

[17] T. Gul, A. Khan, M. Bilal, N. A. Alreshidi, S. Mukhtar, Z. Shah & P. Kumam (2020). Magnetic dipole impact on the hybrid nanofluid flow over an extending surface. *Scientific Reports*, *10*(1), 1–13. https://doi.org/10.1038/s41598-020-65298-1.

[18] S. D. Harris, D. B. Ingham & I. Pop (2009). Mixed convection boundary-layer flow near the stagnation point on a vertical surface in a porous medium: Brinkman model with slip. *Transport in Porous Media*, *77*, 267–285. https://doi.org/10.1007/s11242-008-9309-6.

[19] F. Hoseininejad, S. Dinarvand & M. E. Yazdi (2021). Manninen's mixture model for conjugate conduction and mixed convection heat transfer of a nanofluid in a rotational/stationary circular enclosure. *International Journal of Numerical Methods for Heat & Fluid Flow*, *31*(5), 1662–1694. https://doi.org/10.1108/HFF-05-2020-0301.

[20] N. Iftikhar, A. Rehman, H. Sadaf & S. Iqbal (2019). Study of Al_2O_3/copper–water nanoparticle shape, slip effects, and heat transfer on steady physiological delivery of MHD hybrid nanofluid. *Canadian Journal of Physics*, *97*(12), 1239–1252. https://doi.org/10.1139/cjp-2018-0551.

[21] M. Izady, S. Dinarvand, I. Pop & A. J. Chamkha (2021). Flow of aqueous Fe_2O_3-CuO hybrid nanofluid over a permeable stretching/shrinking wedge: A development on Falkner–Skan problem. *Chinese Journal of Physics*, *74*, 406–420. https://doi.org/10.1016/j.cjph.2021.10.018.

[22] B. Jabbaripour, M. Nademi Rostami, S. Dinarvand & I. Pop (2021). Aqueous aluminium–copper hybrid nanofluid flow past a sinusoidal cylinder considering three-dimensional magnetic field and slip boundary condition. *Proceedings of the Institution of Mechanical Engineers,*

Part E: Journal of Process Mechanical Engineering, pp. 09544089211046434. https://doi.org/10.1177/09544089211046434.

[23] H. Javadi, J. F. Urchueguia, S. S. Mousavi Ajarostaghi & B. Badenes (2021). Impact of employing hybrid nanofluids as heat carrier fluid on the thermal performance of a borehole heat exchanger. *Energies*, *14*(10), Article ID 2892. https://doi.org/10.3390/en14102892.

[24] R. Jusoh, K. Naganthran, A. Jamaludin, M. Ariff, M. Basir & I. Pop (2020). Mathematical analysis of the flow and heat transfer of $Ag - Cu$ hybrid nanofluid over a stretching/shrinking surface with convective boundary condition and viscous dissipation. *Data Analytics and Applied Mathematics*, *1*(1), 11–22. https://doi.org/10.15282/daam.v1i01.5105.

[25] P. Kalidoss, S. G. Venkatachalapathy & S. Suresh (2021). Photothermal performance of hybrid nanofluids with different base fluids for solar energy applications. *Energy Sources, Part A: Recovery, Utilization, and Environmental Effects*, pp. 1–16. https://doi.org/10.1080/15567036.2021.1936697.

[26] A. S. Khan, H. Y. Xu & W. Khan (2021). Magnetohydrodynamic hybrid nanofluid flow past an exponentially stretching sheet with slip conditions. *Mathematics*, *9*(24), 3291. https://doi.org/10.3390/math9243291.

[27] A. Khan, A. Saeed, A. Tassaddiq, T. Gul, P. Kumam, I. Ali & W. Kumam (2021). Bio-convective and chemically reactive hybrid nanofluid flow upon a thin stirring needle with viscous dissipation. *Scientific Reports*, *11*(1), Article ID 8066. https://doi.org/10.1038/s41598-021-86968-8.

[28] U. Khan, Adnan, N. Ahmed, S. T. Mohyud-Din, D. Baleanu, I. Khan & K. S. Nisar (2020). A novel hybrid model for $Cu - Al_2O_3/H_2O$ nanofluid flow and heat transfer in convergent/divergent channels. *Energies*, *13*(7), 1686. https://doi.org/10.3390/en13071686.

[29] L. A. Lund, Z. Omar, I. Khan, A. H. Seikh, E.-S. M. Sherif & K. S. Nisar (2020). Stability analysis and multiple solution of $Cu - Al_2O_3/H_2O$ nanofluid contains hybrid nanomaterials over a shrinking surface in the presence of viscous dissipation. *Journal of Materials Research and Technology*, *9*(1), 421–432. https://doi.org/10.1016/j.jmrt.2019.10.071.

[30] L. A. Lund, Z. Omar, J. Raza & I. Khan (2021). Magnetohydrodynamic flow of $Cu - Fe_3O_4/H_2O$ hybrid nanofluid with effect of viscous dissipation: dual similarity solutions. *Journal of Thermal Analysis and Calorimetry*, *143*, 915–927. https://doi.org/10.1007/s10973-020-09602-1.

[31] E. Magyari & B. Keller (1999). Heat and mass transfer in the boundary layers on an exponentially stretching continuous surface. *Journal of Physics D: Applied Physics*, *32*(5), 577. https://dx.doi.org/10.1088/0022-3727/32/5/012.

[32] J. Merkin (1986). On dual solutions occurring in mixed convection in a porous medium. *Journal of Engineering Mathematics*, *20*(2), 171–179. https://doi.org/10.1007/BF00042775.

[33] M. K. A. Mohamed, H. R. Ong, H. T. Alkasasbeh & M. Z. Salleh (2020). Heat transfer of $Ag - Al_2O_3$/water hybrid nanofluid on a stagnation point flow over a stretching sheet with Newtonian heating. In *Journal of Physics: Conference Series*, volume 1529 pp. 042085. IOP Publishing. https://doi.org/10.1088/1742-6596/1529/4/042085.

[34] G. Morini et al. (2008). Viscous dissipation. In *Encyclopedia of Microfluidics and Nanofluidics*, pp. 2156–2164. Springer,. https://doi.org/10.1007/978-0-387-48998-8_1669.

[35] K. S. Nisar, U. Khan, A. Zaib, I. Khan & D. Baleanu (2020). Exploration of aluminum and titanium alloys in the stream-wise and secondary flow directions comprising the significant impacts of magnetohydrodynamic and hybrid nanofluid. *Crystals*, *10*(8), 679. https://doi.org/10.3390/cryst10080679.

[36] S. Parvin, S. S. P. M. Isa, N. M. Arifin & F. M. Ali (2020). Dual numerical solutions on mixed convection casson fluid flow due to the effect of the rate of extending and compressing sheet–stability analysis. *CFD Letters*, *12*(8), 76–84. https://akademiabaru.com/submit/index.php/cfdl/article/view/3279.

[37] S. Parvin, S. S. P. Mohamed Isa, N. M. Arifin & F. Md Ali (2021). The inclined factors of magnetic field and shrinking sheet in Casson fluid flow, heat and mass transfer. *Symmetry*, *13*(3), 373. https://doi.org/10.3390/sym13030373.

[38] S. S. K. Raju, M. J. Babu & C. Raju (2021). Irreversibility analysis in hybrid nanofluid flow between two rotating disks with activation energy and cross-diffusion effects. *Chinese Journal of Physics*, *72*, 499–529. https://doi.org/10.1016/j.cjph.2021.03.016.

[39] M. G. Reddy, P. Padma & B. Shankar (2015). Effects of viscous dissipation and heat source on unsteady mhd flow over a stretching sheet. *Ain Shams Engineering Journal*, *6*(4), 1195–1201. https://doi.org/10.1016/j.asej.2015.04.006.

[40] G. Revathi, V. S. Sajja, M. J. Babu, C. S. K. Raju, S. Shehzad & C. Bapanayya (2021). Entropy optimization in hybrid radiative nanofluid ($CH_3OH + SiO_2 + Al_2O_3$) flow by a curved stretching sheet with cross-diffusion effects. *Applied Nanoscience*, *13*, 337–351. https://doi.org/10.1007/s13204-021-01679-w.

[41] N. C. Roy, L. K. Saha & M. Sheikholeslami (2020). Heat transfer of a hybrid nanofluid past a circular cylinder in the presence of thermal radiation and viscous dissipation. *AIP Advances*, *10*(9), 095208. https://doi.org/10.1063/5.0021258.

[42] S. Saranya, Q. M. Al-Mdallal & S. Javed (2021). Shifted legendre collocation method for the solution of unsteady viscous-ohmic dissipative hybrid ferrofluid flow over a cylinder. *Nanomaterials*, *11*(6), 1512. https://doi.org/10.3390/nano11061512.

[43] M. Shoaib, M. A. Z. Raja, M. T. Sabir, M. Awais, S. Islam, Z. Shah & P. Kumam (2021). Numerical analysis of 3-D MHD hybrid nanofluid over a rotational disk in presence of thermal radiation with Joule heating and viscous dissipation effects using Lobatto IIIA technique. *Alexandria Engineering Journal*, *60*(4), 3605–3619. https://doi.org/10.1016/j.aej.2021.02.015.

[44] S. Suresh, K. Venkitaraj, P. Selvakumar & M. Chandrasekar (2012). Effect of $Al_2O_3 - Cu$/water hybrid nanofluid in heat transfer. *Experimental Thermal and Fluid Science*, *38*, 54–60. https://doi.org/10.1016/j.expthermflusci.2011.11.007.

[45] B. Venkateswarlu & P. V. Satya Narayana (2021). $Cu-Al_2O_3/H_2O$ hybrid nanofluid flow past a porous stretching sheet due to temperatue-dependent viscosity and viscous dissipation. *Heat Transfer*, *50*(1), 432–449. https://doi.org/10.1002/htj.21884.

[46] I. Waini, A. Ishak & I. Pop (2019). Hybrid nanofluid flow and heat transfer past a permeable stretching/shrinking surface with a convective boundary condition. In *Journal of Physics: Conference Series*, volume 1366 pp. 012022. IOP Publishing. https://dx.doi.org/10.1088/1742-6596/1366/1/012022.

[47] I. Waini, A. Ishak & I. Pop (2019). Hybrid nanofluid flow and heat transfer over a nonlinear permeable stretching/shrinking surface. *International Journal of Numerical Methods for Heat & Fluid Flow*, *29*(9), 3110–3127. http://dx.doi.org/10.1108/HFF-01-2019-0057.

[48] I. Waini, A. Ishak & I. Pop (2020). Mixed convection flow over an exponentially stretching/shrinking vertical surface in a hybrid nanofluid. *Alexandria Engineering Journal*, *59*(3), 1881–1891. https://doi.org/10.1016/j.aej.2020.05.030.

[49] P. Weidman, D. Kubitschek & A. Davis (2006). The effect of transpiration on self-similar boundary layer flow over moving surfaces. *International Journal of Engineering Science*, *44*(11-12), 730–737. https://doi.org/10.1016/j.ijengsci.2006.04.005.

[50] N. Zainal, R. Nazar, K. Naganthran & I. Pop (2021). Viscous dissipation and MHD hybrid nanofluid flow towards an exponentially stretching/shrinking surface. *Neural Computing and Applications*, *33*, 11285–11295. https://doi.org/10.1007/s00521-020-05645-5.

[51] M. Zufar, P. Gunnasegaran, H. M. Kumar & K. C. Ng (2020). Numerical and experimental investigations of hybrid nanofluids on pulsating heat pipe performance. *International Journal of Heat and Mass Transfer*, *146*, Article ID 118887. https://doi.org/10.1016/j.ijheatmasstransfer.2019.118887.